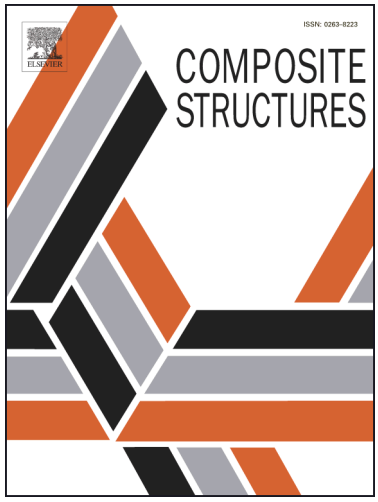

Optimization of GFRP reinforcement in precast segments for metro tunnel lining

Angelo Caratelli, Alberto Meda, Zila Rinaldi, Simone Spagnuolo, Giona Maddaluno

PII: S0263-8223(17)31826-3
DOI: http://dx.doi.org/10.1016/j.compstruct.2017.08.083
Reference: COST 8841

To appear in: *Composite Structures*

Received Date: 6 June 2017
Revised Date: 17 August 2017
Accepted Date: 29 August 2017

Please cite this article as: Caratelli, A., Meda, A., Rinaldi, Z., Spagnuolo, S., Maddaluno, G., Optimization of GFRP reinforcement in precast segments for metro tunnel lining, *Composite Structures* (2017), doi: http://dx.doi.org/10.1016/j.compstruct.2017.08.083

Optimization of GFRP reinforcement in precast segments for metro tunnel lining

Angelo Caratelli[1], Alberto Meda[1], Zila Rinaldi[1*]; Simone Spagnuolo[1]; Giona Maddaluno[2]

[1] University of Rome Tor Vergata, Via del Politecnico 1, 00133 Rome, Italy

[2] ATP s.r.l. Casa Pagano 31, 84012 Angri (SA) Italy

*** Corresponding author:**

Zila Rinaldi, University of Rome Tor Vergata, Via del Politecnico, 1, 00133 Rome, Italy

tel. +39-0672597080, email: rinaldi@ing.uniroma2.it

Abstract

The possibility of replacing the traditional steel reinforcement with glass fiber reinforced polymer (GFRP) cages in precast concrete tunnel segmental lining has been shown by the authors in previous papers. The use of GFRP rebars as structural reinforcement in precast tunnel segments, allows several advantages in terms of structural durability or in cases of temporary lining that will have to be demolished later. Furthermore, this reinforcement type can be a suitable solution to create dielectric joints, ensuring the interruption of possible stray currents, which often lead to corrosion problems. Nevertheless, this peculiar application requires curvilinear shape of the reinforcement, and then different production process and rebar geometries. In the present work, a suggestion for the optimization of the GFRP reinforcement for tunnel segment is given. Four different GFRP cage typologies are analysed and applied as a reinforcement in full-scale tunnel segments. Both bending and point load tests are developed and the structural performances of the specimens are compared and discussed. Finally, the best solution, in terms of cost-benefit analysis is proposed.

keywords: Glass FRP bars, tunnel lining segments, GFRP cage prototypes, Full-scale tests

Introduction

The application of glass fiber reinforced polymer (GFRP) reinforcement in concrete structures, has encountering an increasing interest worldwide, for several applications in civil engineering. The main advantages of the GFRP material are the lightweight, the high tensile strength and non-corrosive properties (Uomoto et al. 2002, Chen et al. 2007). Furthermore, it is worth highlighting that GFRP material is non-conductive for electricity and non-magnetic. Nevertheless, the GFRP reinforcement may suffer static fatigue when subjected to high-level long-term tensile stresses (Almussalam et al., 2006) and the structural performances can be affected by the low value of the Young's modulus and by the poor bond behaviour (Cosenza et al., 1997, Yoo et al., 2015). Finally, the material durability can be improved and controlled through a suitable choice of the composite constituents (Micelli, Nanni 2004, Chen et al., 2007). The application of GFRP reinforcement as a substitute of the traditional steel rebars in the precast segments of tunnel lining, could represent a suitable solution to the challenges of underground construction in terms of maintenance cost and durability. In underground structures mechanically excavated by means of tunnel boring machine (TBM), the lining is composed of precast elements, placed by the TBM during the excavation process and used as reaction elements during the advancing phase (Meda et al., 2016). This peculiar application appears suitable for the adoption of GFRP reinforcement for different reasons. First of all, it allows to overcome the problem of the structural durability, often jeopardized by the steel reinforcement corrosion. Furthermore, the use of this non-corrosive reinforcement in tunnel segments allows reducing the concrete cover that is usually a weak point for this kind of structure, since it can crash during handling or due to TBM thrusts. Due to the further property of being chemical inert, the GFRP reinforcement provides a low conductivity against the stray currents and is adequate for creating dielectric joints in tunnels (Caratelli et

al. 2016, Spagnuolo et al. 2017). Indeed, a tunnel ring made with precast GFRP reinforced segments breaks the electrostatic continuity of the ordinary cages (reinforced with steel) and guarantees an effective remedy to the problem of stray currents and corrosion resulting therefrom.

Finally, the GFRP reinforcement solution appears very interesting for the parts of the tunnel that have to be eventually removed (niches, vent channels, openings and stations), due to the easiness of demolition and disposal.

The mechanical properties of straight GFRP bars, are nowadays well known (Nanni, 1993, Alsayed et al., 2000; Pecce et al., 2000; Ashour, 2006; Aiello et al. 2007, Miàs et al., 2013, Adam et al., 2015, Coccia et al., 2017), and codified (CSA, 2002, ACI 440.1R-15, 2015; CNR DT 203-2006, 2007). Nevertheless, for application in tunneling lining, the GFRP reinforcement should present a curvilinear configuration. At this aim, both the geometry and the manufacturing process are different from the ones of the straight rebars.

The results of experimental full-scale tests on precast concrete segments reinforced with GFRP bars (Spagnuolo et al. 2014, Spagnuolo et al. 2017, Caratelli et al. 2016) showed the effectiveness of this solution, able to satisfy the requested capacity. Main aim of this paper is the optimization of the GFRP reinforcement geometry in concrete precast segments, for improving the crack control, in the perspective of a cost-benefit analysis.

Four GFRP reinforcement cage prototypes are studied and produced. Both flexural and point-load tests, simulating the bending behavior and the TBM thrust phase, are developed on full-scale segments, with typical geometries of metro linings. The obtained results are discussed and compared with the ones obtained on traditionally steel reinforced elements. Finally, the best solution in terms of cost-benefit analysis is proposed.

1. EXPERIMENTAL PROGRAM

The experimental program is developed with reference to structural elements belonging to a typical metro tunnel.

Full scale segments were made with different typologies of reinforcement (four different types of GFRP reinforcement plus a reference segment with traditional steel reinforcement). For every reinforcement typology, two segments were cast at the Laboratory of Material and Structures of the University of Rome Tor Vergata. One segment was subjected to bending whereas the other was tested simulating the TBM thrust. As a consequence, one segment was tested for every reinforcement typology and every testing set-up, for a total of ten full-scale tests.

1.1 Segment geometry

The analyzed metro tunnel has an internal diameter of 5800 mm and a lining thickness equal to 300 mm (Figure 1). The lining precast concrete segment has a width of 1420 mm, as shown in Figure 2.

1.2 Curvilinear GFRP reinforcement

For typical applications, the GFRP reinforcement consists of straight bars manufactured by means of well-established pultrusion industrial technology. In underground tunnels, reinforcements with curvilinear configuration is required and the pultrusion process cannot be adopted. At the aim, a modified pultrusion process named “pull-forming”, has been developed, able to produce curvilinear bars with a constant and large curvature radius. The behavior of precast concrete segments with GFRP reinforcement made with the pull-forming technology is reported in Caratelli et al. (2016) and Spagnuolo et al. (2017). The reinforcement cage consisted of longitudinal coupled curvilinear bars (intrados/extrados) closed to the edges by means of “C” shape pieces (Figure 3a). In this case, the assembling of

the cage can become difficult and expensive. In fact, since a thermosetting resin is used as matrix for the GFRP composite, from technological point of view, the curvilinear bars cannot be bended in plastic way and, furthermore, cannot be welded. Additionally, many ligatures by hands would be necessary, taking much time for their manufacturing. In this research, a new manufacturing technology has been developed, able to realize cages composed of GFRP "closed-rings", as shown in Figure 3b.

In the light of this new technological process, different GFRP cages prototypes have been designed, considering technical, commercial and technological feasibility.

These aspects are the basis of engineering industrialization, leading to create a technological system that can be standardized, in order to maximize the compatibility, interoperability, safety, repeatability, and quality.

1.3 Reinforcement cages: steel reference and GFRP prototypes

Starting from a traditional steel reinforcement (SR) cage, used as reference, four different GFRP reinforcement cages were designed and realized.

The reference steel reinforcement (SR) consists of 12 Ø12 longitudinal rebars both intrados and extrados surface, closed to the ends by means of two "C" shaped stirrup. The transverse reinforcement is made with straight rebars closed by means of different "C" shaped stirrups. Minimum concrete cover is equal to 50 mm (Figure 4a).

The first solution for GFRP type concerns the closed "Ring Reinforcement" (GFRP-RR), as mentioned above. The main longitudinal GFRP reinforcement consists of 12 closed-rings equals to 12 mm equivalent diameter. As well as for the longitudinal reinforcement, transverse reinforcement (stirrups) is made of "closed-rings" with cross-sectional area equal to an equivalent round bar of 8 mm in diameter (Figure 4b).

The final cage is made by means of interlinked closed-rings (longitudinal/transversal): it is an innovative solution that would facilitate the assembly operation.

The second GFRP cage solution, is a "Lattice Reinforcement" (GFRP-LR). It is a combination of reinforcement curvilinear bars, which are interlinked by means of lattice structures (Figure 4c). In the main direction, the closed-rings are replaced with bended rebars (staggered between them) and lattice reinforcements. The GFRP reinforcement cage consists of 9 Ø16 and 8 Ø16 curvilinear bars in intrados and extrados surface respectively, with minimum concrete cover of 50 mm. Furthermore, 12Ø8 lattice reinforcements are interspersed with the curvilinear bars (Figure 4c - Lattice #1 to # 12).

In the transverse direction, besides the stirrups (14 bars with diameter of 8 mm), the lattice structures (characterized by the same stirrups diameter) are placed (Figure 4c - #19). Due to the above described elements, a complex and rigid system has been achieved.

The third GFRP solution is a "Wirenet Reinforcement" (GFRP-WR). In this case a wirenet is placed in the extrados side with a mesh of 150×140 mm and diameter of 13 and 8 mm respectively. The wirenet in intrados has a mesh of 140×140 mm and diameter of 13 and 8 mm respectively. "C" shaped stirrups close the edges with equivalent bars of diameter from 8 to 14 mm and 110 Ø8 "pins" have the task of confining and spacing the two wirenets. Figure 4d shows GFRP-WR reinforcement details.

Finally, a further solution was considered, named GFRP-RR(+B) obtained from the GFRP-RR prototype, through a sand coating of the closed ring reinforced reinforcement. (Figure 12), with the aim of improving the bond properties.

1.4. Materials

All GFRP reinforcement cages were made with E-CR glass and vinyl ester resin.

The properties of the GFRP reinforcement constituents are illustrated in Table 1. In the same table the concrete average strength, measured on six 150x150x150mm cubes, and the yielding and ultimate stress of the steel rebars for the SR solution, are summarized.

2. TESTING SET UP

Two different testing set-up were carried out:

- a bending test aiming to represent the transient load conditions;
- a point load test aiming to simulate the TBM thrust.

2.1. Bending test set up

The test aims verifying the segment performance under prevalent bending moment action, and then it is also representative of the provisional loading stages as demoulding, storage and handling.

The typical testing set-up (Caratelli et., 2002, Caratelli et al. 2016). is shown in Figure 5. The segment was placed on roller supports with a span (L) equal to 2.0 m (Figure 6). A frame system was used to distribute the load along the transverse direction (Figure 7 a).

Three wire transducers (WT) were used for measuring the vertical displacement, while two linear variable differential transformer (LVDTs) were applied in order to measure the crack opening. Both wires and LVDTs were placed on intrados surface (Figure 7 b).

2.2. Point load test set up

The point load test set-up is shown in Figure 8. The point loads, simulating the TBM thrust, are applied on the segment, adopting the actual pad configuration and geometry used by the TBM (Figure 8 a, b, c). Two 2000 kN hydraulic jacks push on each pad (maximum 4000 kN per pad), for a total maximum force of 12.000 kN.

A uniform support is considered, as the segment is placed on a stiff beam suitably designed (Figure 8 a, b).

For each loading steel pad, a couple of potentiometers (placed on intrados and extrados segment surface respectively) with a length equal to 1420 mm were adopted to measure the

vertical displacements (Figure 8 f). Furthermore, two LVDTs, used to measure possible cracks opening, were placed each between a pair of steel pads (Figure 8 d).

Scheme of the crack pattern at different loading steps were recorded, as well as the opening of the main cracks by means of a crack width gauge card.

Two complete loading-unloading cycles, with steps of about 250 kN were carried out, and, in particular, as summarized in Figure 9:

- First cycle: 0-1580 kN (loading cycle up to service load); and
- Second cycle: 0-2670 kN (loading cycle up to the maximum TBM thrust load).

3. TEST RESULTS

3.1. Bending test results

The results, expressed in terms of load versus midspan displacement, obtained from the full-scale tests carried out on the reference steel reinforced element (SR) and the GFRP reinforced segments without sand coating (GFRP-RR, GFRP-LR and GFRP-WR) are compared in Figure 10. The main outcomes are summarized in Table 2, including the load at first crack (P_{crack}), the maximum crack width (w_{crack}), the maximum load (P_{max}), the maximum midspan deflection (δ_{max}), the midspan deflection at steel yielding (δ_y) for SR segment, and deflection when the stiffness drastically changes (δ_l) for GFRP reinforced elements. Furthermore, an indication of the ductility factor (μ), defined as the ratio (δ_{max}/δ_y) for traditional steel reinforced segment and as the ratio (δ_{max}/δ_l) for the GFRP reinforced one, is given. The observed failure mode is also pointed out.

After first cracks, several cracks developed in all the segments as shown in Figure 11, where the complete crack patterns and widths are plotted for all the examined cases.

Because of higher Young's modulus of steel rebars with respect to GFRP ones, the SR segment showed a behavior stiffer than the GFRP ones. Figure 11 points out how the crack patterns are comparable for each segment tested, regardless of the reinforcement adopted. In all cases analysed, the failure occurred for the attainment of the tensile strength in the intrados reinforcement.

As already found in (Spagnuolo et al. 2017), all precast concrete segments shown a comparable structural behavior in terms of maximum displacements, despite of the brittleness of the GFRP reinforcement.

Looking at the results, whilst the GFRP-WR segment showed a failure load equal to the reference SR one, the other two prototypes, GFRP-RR and GFRP-LR, exhibited significantly higher failure loads, with increases of about 32.7% and 16.7% respectively, with respect to the reference element.

In the light of the results obtained and taking into account the three manufacturing process aspects, mentioned above (technical feasibility, commercial feasibility and technological feasibility), the GFRP-RR represents the best solution among the prototypes tested.

Nevertheless, as expected, higher cracks width were measured in the GFRP reinforced element, with respect to the traditional reinforced one (SR), as shown in Table 2 and Figure 11.

In order to enhance this behavior by improving the bond performances, a sand coating of the GFPR ring reinforcement was carried out, and a new segment named GFRP-RR(+B) was cast and tested. The measured load-displacement diagram is shown in Figure 13 and compared with the GFRP-RR typology. The main outcomes are further shown and compared in Table 3, including: load at first crack (P_{crack}), maximum crack width at first crack (w_{crack}). Furthermore, crack width reduction (R_w) is included.

The coating treatment, besides increasing the load at first crack, led to a reduction of about 70% the width crack, passing from 0.50 mm to 0.15 mm.

Figure 14 shows, from a quality point of view, the crack patterns comparison between the solutions. In both cases, several cracks have been developed. The sand coating of the GFRP-RR(+B) segment led to more widespread cracks (Figure 14 b) with lesser width compared the same solution without surface treatment (Figure 14 a).

3.2. Point load test results

The point load test results, in terms of crack pattern for SR and GFRP reinforcement typology without sand coating, and for each load step, is shown in Figure 15.

In all the analysed cases, the first cracks opened between the load pads, and extended their length, at the load increase, in the whole element height. For high load values, close to the maximum one, bursting cracks opened under the steel pads.

In Table 4 the maximum crack width (w_{crack}) measured in each cycle considered, is summarized. Furthermore, the maximum crack width (w_{max}) suggested by (CNR-DT203, 2007) for concrete structures with GFRP reinforcement, is shown.

The maximum value of the crack width, under the serviceability and maximum loads, are higher in GFRP specimens, if compared to steel reinforced element ones.

Once again, as shown in Table 4, the GFRP-RR prototype represents the best solution among those under evaluation. This is confirmed, not only during the loading steps in which the crack width are smaller than those observed on GFRP-LR and GFRP-WR but, looking at the crack width at the end of the test, when the load was removed, the cracks are within the limitation imposed by CNR (CNR DT 203-06 2006).

Finally, the segment reinforced with sand coating rings reinforcement, GFRP-RR(+B), was cast and tested (Figure 16). Looking at the results (Table 4), in term of maximum crack width, the sand coating increased the segment performance leading to cracks width

decreasing from 0.40 mm (without bond) to 0.25 mm (with bond) with a reduction of 37.5 percentage points.

Conclusions

The results of experimental full-scale test on metro tunnel segments with GFRP reinforcement are presented and discussed. Both flexural and TBM thrust tests were carried out.

Three different typologies of GFRP reinforcement were designed and realized. The obtained results were discussed and compared with the one measured on a reference segment with traditional steel reinforcement.

The first solution, named GFRP-RR consists of closed "Ring Reinforcement" for both longitudinal and transverse reinforcement; the second one, GFRP-LR, is a "Lattice Reinforcement" and it is a combination of curvilinear bars, which are interlinked by means of lattice structures. The third prototype is a "Wirenet Reinforcement" (GFRP-WR), in which the reinforcement cage consists of a wire net in extrados and intrados with "C" shaped stirrups. Finally, in order to better control the crack pattern and width, a solution obtained through a sand coating of the closed ring reinforcement, named GFRP-RR (+B) was produced and tested.

If compared to the behavior of a traditional steel reinforced segments, the obtained results show the effectiveness of the proposed reinforcement with GFRP bars in tunnel linings. In particular, based on the experimental structural behaviors, it can be concluded that, with reference to both the performances under flexure and TBM thrust, the best solution appears the Closed Ring Reinforcement (RR). A further enhancement, in terms of crack width, can be obtained if a sand coating is carried out. Nevertheless, if no severe requirement, in term of crack openings for high load levels are imposed in the design process, the Closed Ring Reinforcement appears to be the most suitable solution.

Acknowledgement

The authors gratefully acknowledge (1) European commission – Executive Agency for Small and Medium-sized Enterprises (EASME) H2020 SME for funding the research program; (2) ATP S.r.l. for the support provided.

This project has received funding from the European Union's Horizon 2020 research and innovation programme under grant agreement No 672267.

This document reflects only the author's view and the Agency is not responsible for any use that may be made of the information it contains.

References

ACI (American Concrete Institute). (2015). "Guide for the design and construction of concrete reinforced with FRP bars". ACI 440.1R-15, Farmington Hills, MI.

Adam, M. A., Said, M., Mahmoud, A. A., Shanour, A. S. (2015). "Analytical and experimental flexural behavior of concrete beams reinforced with glass fiber reinforced polymers bars." Construction and Building Materials; Vol. 84, June 2015, pp. 354-366.

Aiello M. A., Leone, M., Pecce, M. (2007). "Bond Performances of FRP Rebars-Reinforced Concrete" Journal of Materials in Civil Engineering; Vol.19 Issue 3 (March 2007). DOI: http://dx.doi.org/10.1061/(ASCE)0899-1561(2007)19:3(205).

Almusallam, T., H., Al-Salloum, Y., A. (2006). "Durability of GFRP Rebars in Concrete Beams under Sustained Loads at Severe Environments." Journal of Composite Materials, Vol. 40, No 7, pp. 623-637.

Alsayed, S.H., Al-Salloum, Y.A., Almusallam, T.H. (2000). "Performance of glass fiber reinforced plastic bars as a reinforcing material for concrete structures." Composite Part B: Engineering, Vol. 31, No 6-7, pp. 555-567.

Ashour, A. F. (2006). "Flexural and shear capacities of concrete beams reinforced with GFRP bars." Construction and Building Materials; Vol. 20, Issue 10, pp. 1005-1015.

Caratelli, A., Meda, A., Rinaldi, Z. (2012). "Design according to MC2010 of a fibre-reinforced concrete tunnel in Monte Lirio, Panama." Structural Concrete, Vol. 13, No 3, September, pp. 166-173.

Caratelli, A., Meda, A., Rinaldi, Z., Spagnuolo S. (2016). "Precast tunnel segments with GFRP reinforcement". Tunnelling and Underground Space Technology vol. 60 (Nov. 2016) pp. 10–20.

Chen, Y., Davalos, J. F., Kim, H-Y. (2007). "Accelerated aging tests for evaluations of durability performance of FRP reinforcing bars for concrete structures." Composite Structures, Vol. 78, March, pp. 101–111.

CNR (Italian National Research Council). (2006). "Guide for the Design and Construction of Concrete Structures Reinforced with Fiber-Reinforced Polymer Bars." CNR DT 203-2006, Rome, Italy.

Coccia S., Meda, A., Rinaldi, Z. Spagnuolo, S. 2017. Influence of GFRP skin reinforcement on the crack evolution in RC ties. Composites Part B. Vol. 119, 15 June 2017, Pages 90-100doi.org/10.1016/j.compositesb.2017.03.048.

Cosenza, E., Manfredi, G., and Realfonzo, R. (1997). "Behavior and Modeling of Bond of FRP Rebars to Concrete." Journal of Composites for Construction, Vol. 1, No. 2, May, pp. 40-51.

CSA (Canadian Standards Association). (2002). "Design and Construction of Building Components with Fiber Reinforced Polymers." CAN/CSA-S806-02, Toronto, Ontario. Canada.

Meda, A., Rinaldi, Z., Caratelli, A., Cignitti, F. (2016). "Experimental investigation on precast tunnel segments under TBM thrust action." Engineering Structures Vol. 119, July 2016, pp. 174-185. DOI:10.1016/j.engstruct.2016.03.049.

Miàs, C., Torres, LI, Turon, A., Sharaky, I. A. (2013). "Effect of material properties on long-term deflections of GFRP reinforced concrete beams." Construction and Building Materials Vol. 41, April 2013, pp. 99-108.

Micelli, F., Nanni, A. (2004). "Durability of FRP rods for concrete structures." Construction and Building Materials Vol. 18, No 7, September, pp. 491–503.

Nanni, A. (ed.). (1993). "Fiber-Reinforced-Plastic (GFRP) Reinforcement for Concrete Structures: Properties and applications." Elsevier Science. Developments in Civil Engineering, 42, p.450.

Pecce M, Manfredi G, Cosenza E. 2000. Experimental response and code models of GFRP RC beams in bending. ASCE J Compos Construct. 2000. 4 (4):182–90.

Spagnuolo, S., Meda, A., Rinaldi, Z. (2014). "Fiber glass reinforcement in tunneling applications." Proc. The 10th *fib* international PhD symposium in civil engineering. 21-23 July, Québec, Canada, pp. 85-90.

Spagnuolo, S., Meda, A., Rinaldi, Z., Nanni, A. (2017). Precast Concrete Tunnel Segments with GFRP Reinforcement. Journal of Composites for Construction. ASCE. DOI: 10.1061/(ASCE)CC.1943-5614.0000803.

Uomoto, T., Mutsuyoshi, H., Katsuki, F., Misra, S. (2002). "Use of Fiber Reinforced Polymer Composites as Reinforcing Material for Concrete." J. Mat Civil Eng, ASCE, 14(3):191-209.

Yoo, D-Y., Kwon K-Y., Park J-J., Yoon Y-S. (2015). "Local bond-slip response of GFRP rebar in ultra-high-performance fiber-reinforced concrete." Composite Structures Vol. 120, pp. 53–64.

Figures

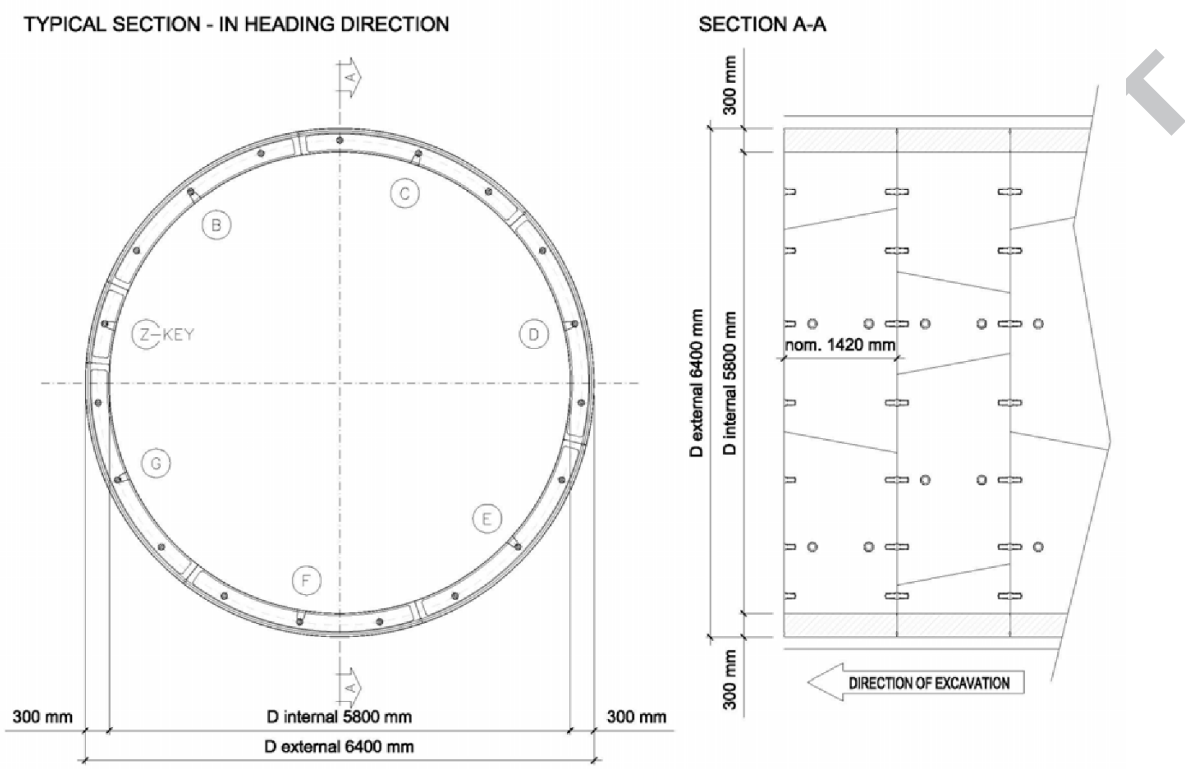

Figure 1. Metro tunnel geometry.

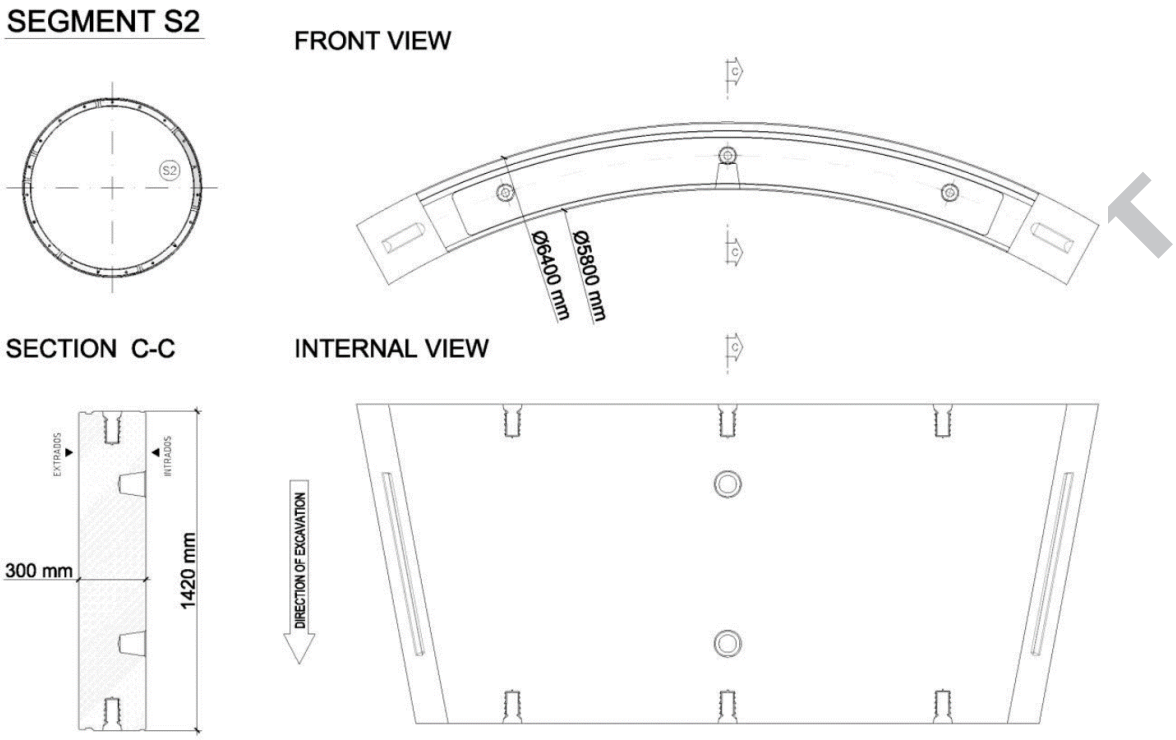

Figure 2. Segment geometry.

Figure 3. a) Traditional GFRP longitudinal reinforcement; b) New GFRP "closed-rings" reinforcement.

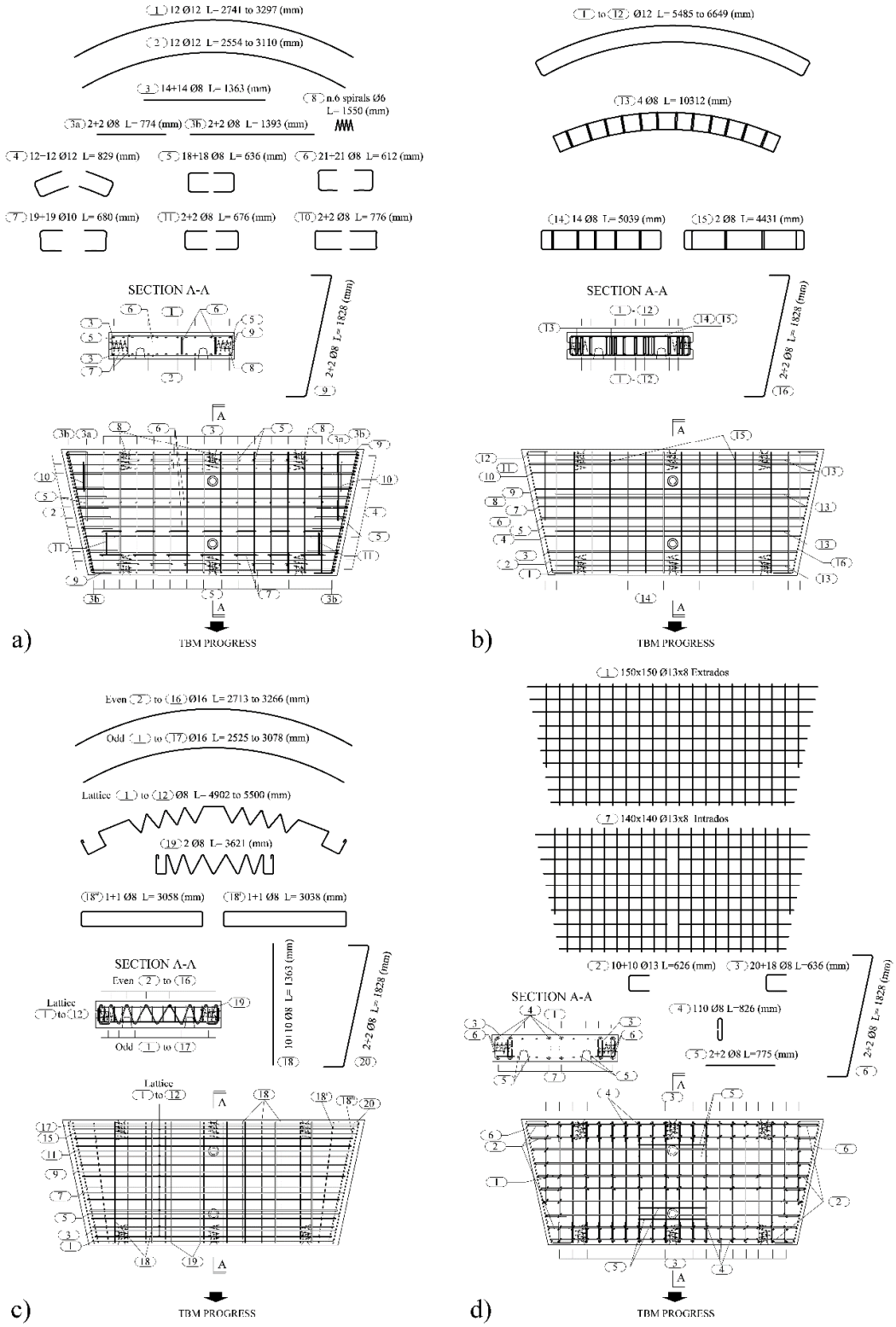

Figure 4. Reinforcement details: a) SR; b) GFRP-RR; c) GFRP-LR; and d) GFRP-WR.

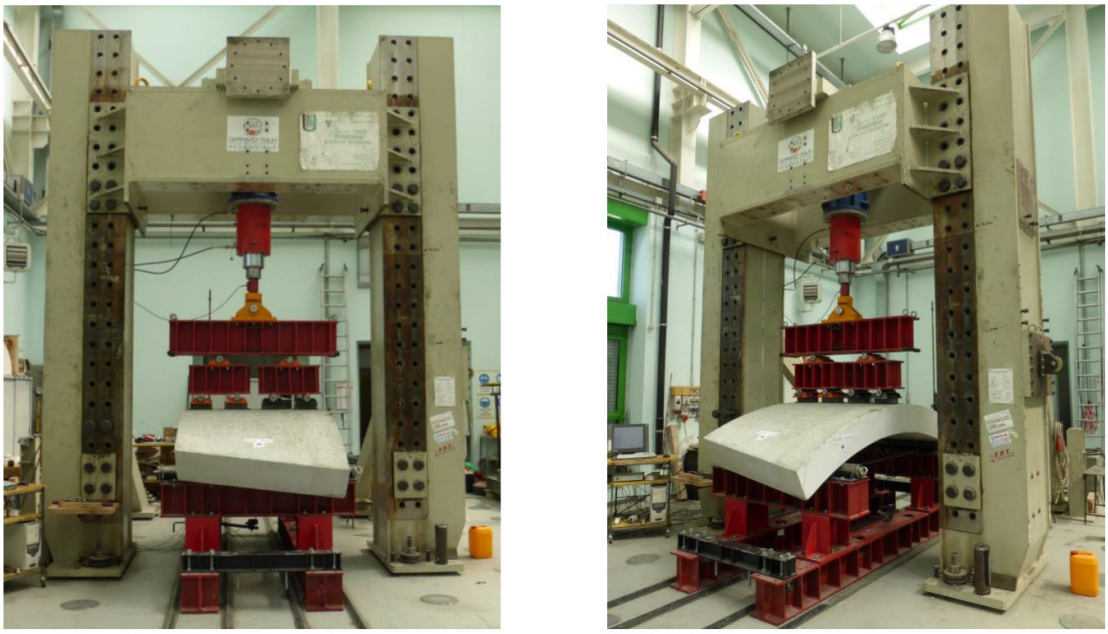

a) b)

Figure 5. Bending test: a) front view; b) lateral view.

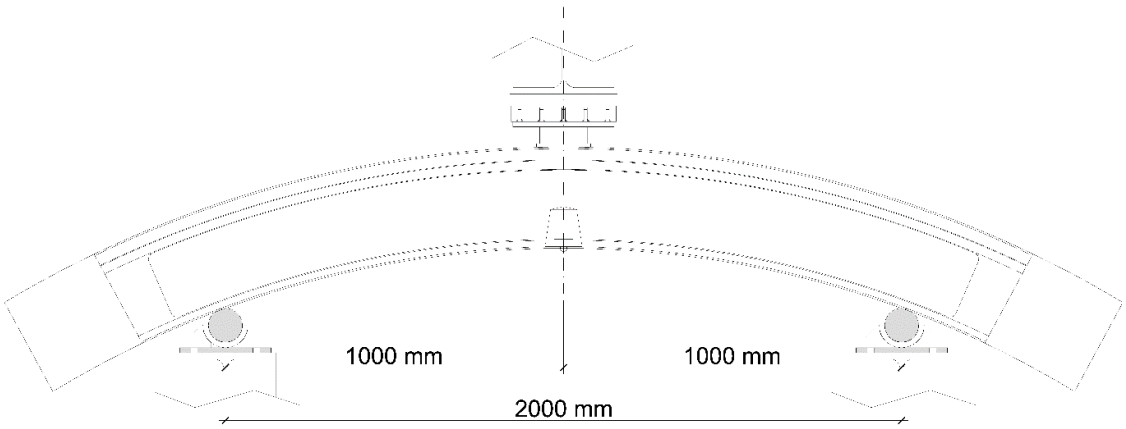

Figure 6. Position of the precast concrete segment on the supports.

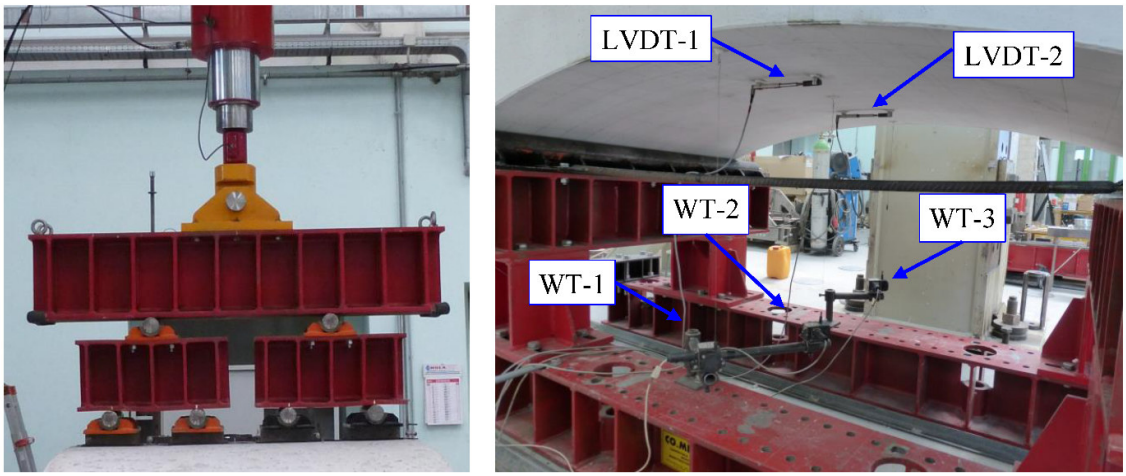

a) b)

Figure 7. Bending test set up: a) Frame system for distributing the load along the midspan width; and b) Instrumentation - wire transducers (WT) and LVDTs.

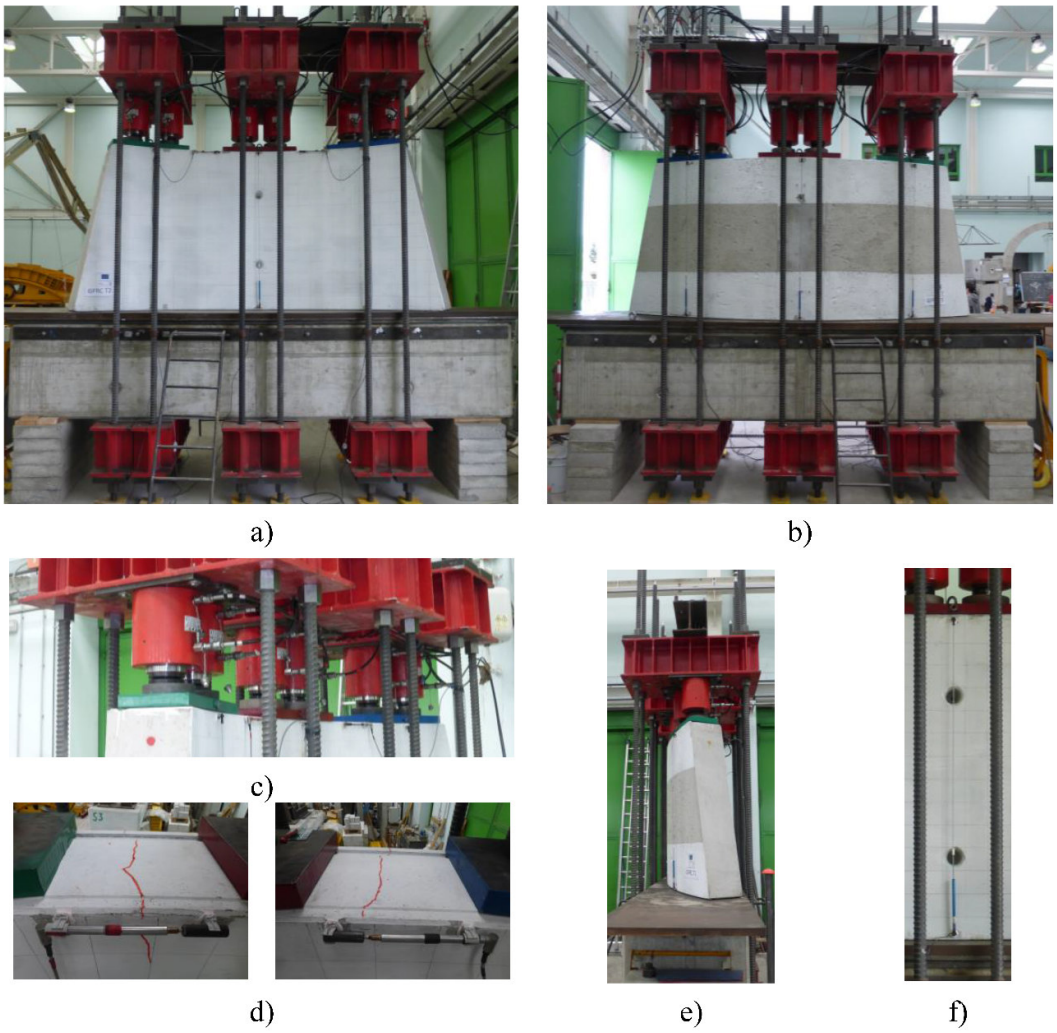

Figure 8. Point load test set up: a) intrados view; b) extrados view; c) loading steel pad view; d) LVDTs between the steel pads (intrados surface); e) lateral view; and f) potentiometer detail.

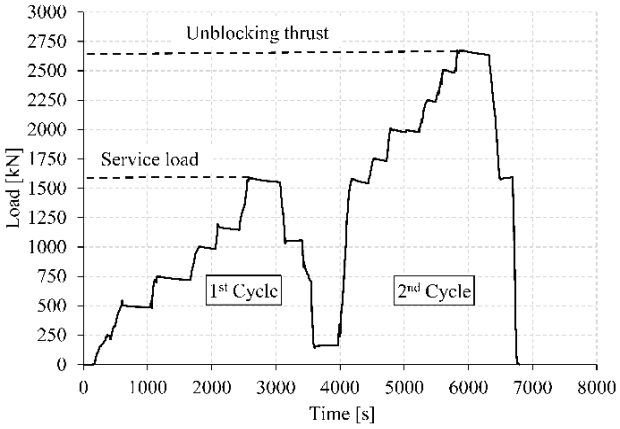

Figure 9. Point load test: loading-unloading cycles

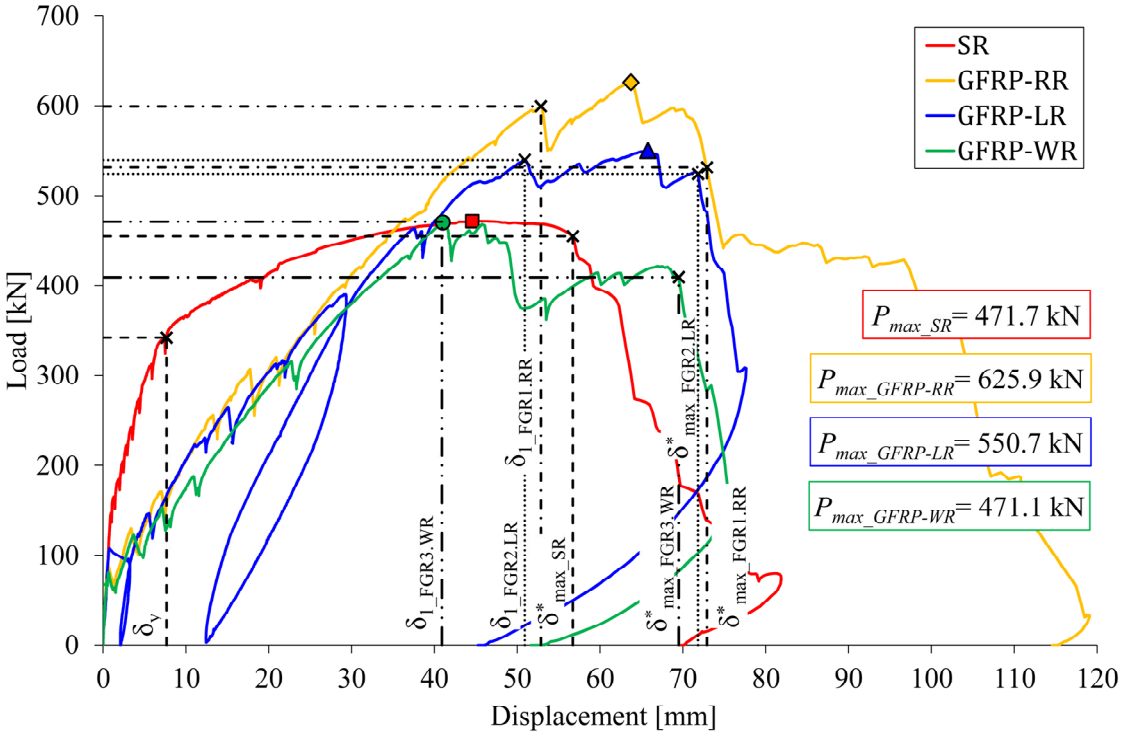

Figure 10. Bending test results: load versus displacement comparison.

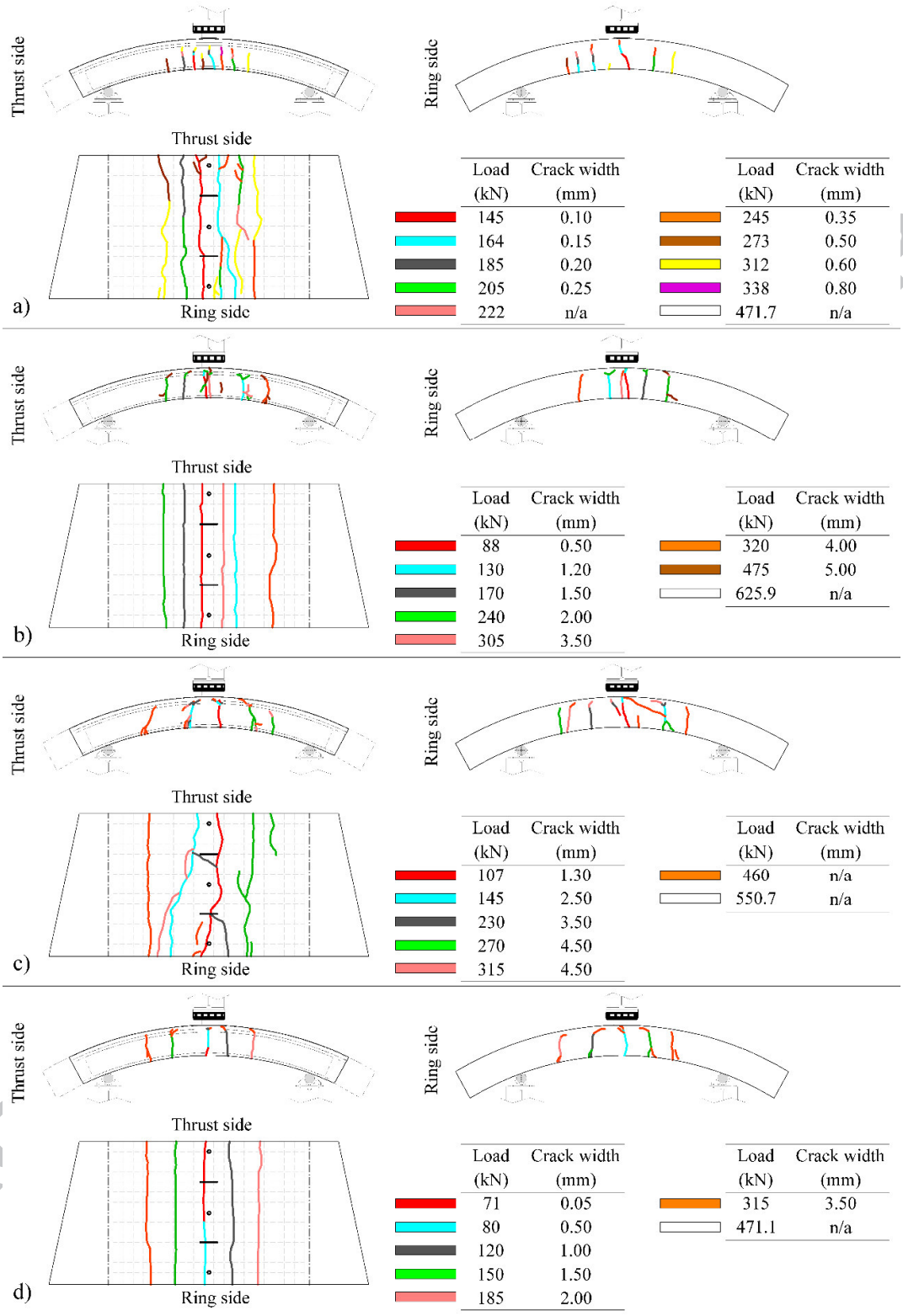

Figure 11. Bending test results: crack pattern. a) SR; b) GFRP-RR; c) GFRP-LR; and d) GFRP-WR.

Figure 12. GFRP-RR(+B)

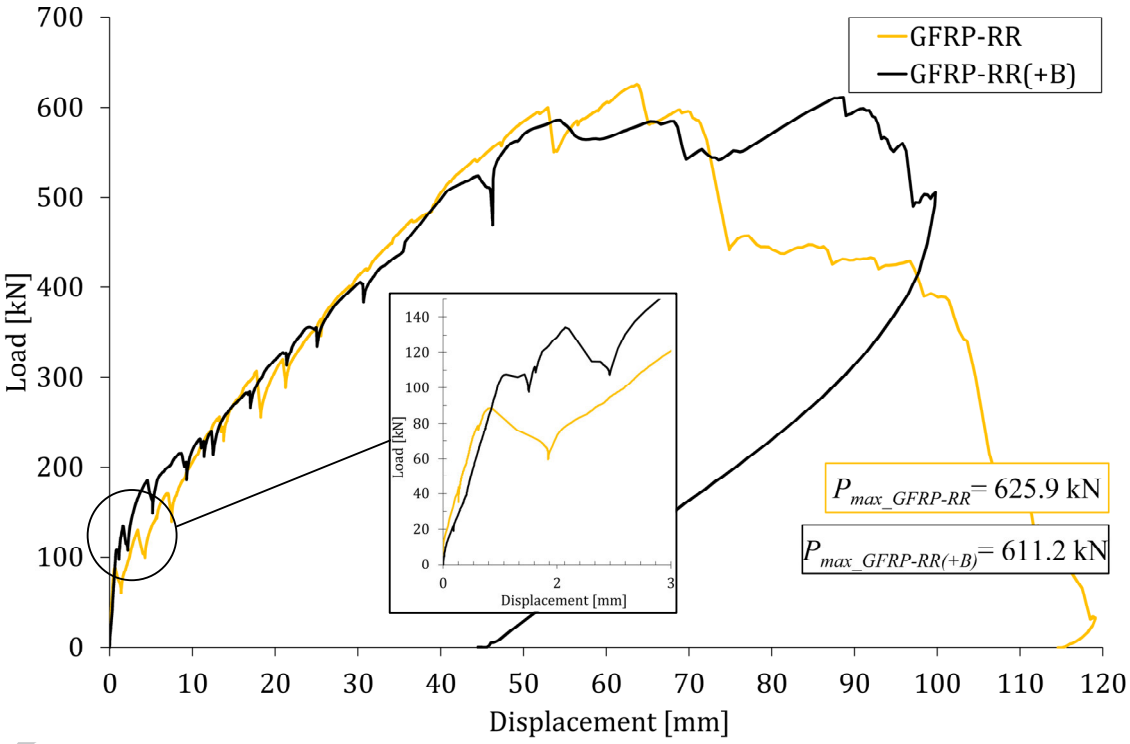

Figure 13. Comparison between GFRP-RR and GRRP-RR(+ B)

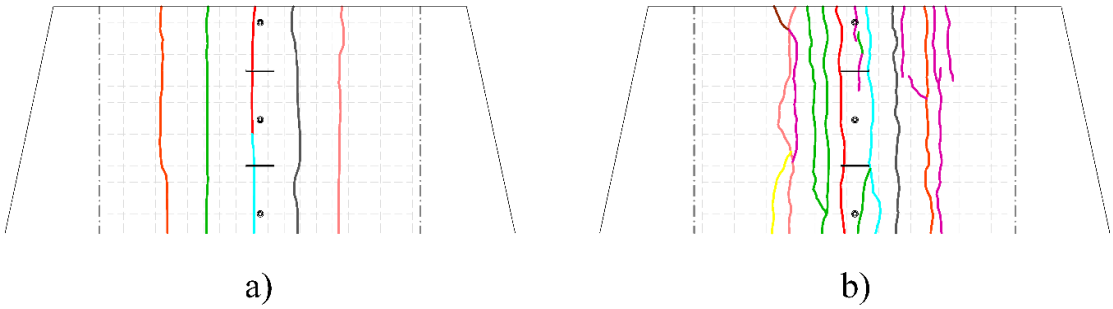

Figure 14. Bending test: crack pattern comparison. a) GFRP-RR; and b) GFRP-RR(+ B) segment.

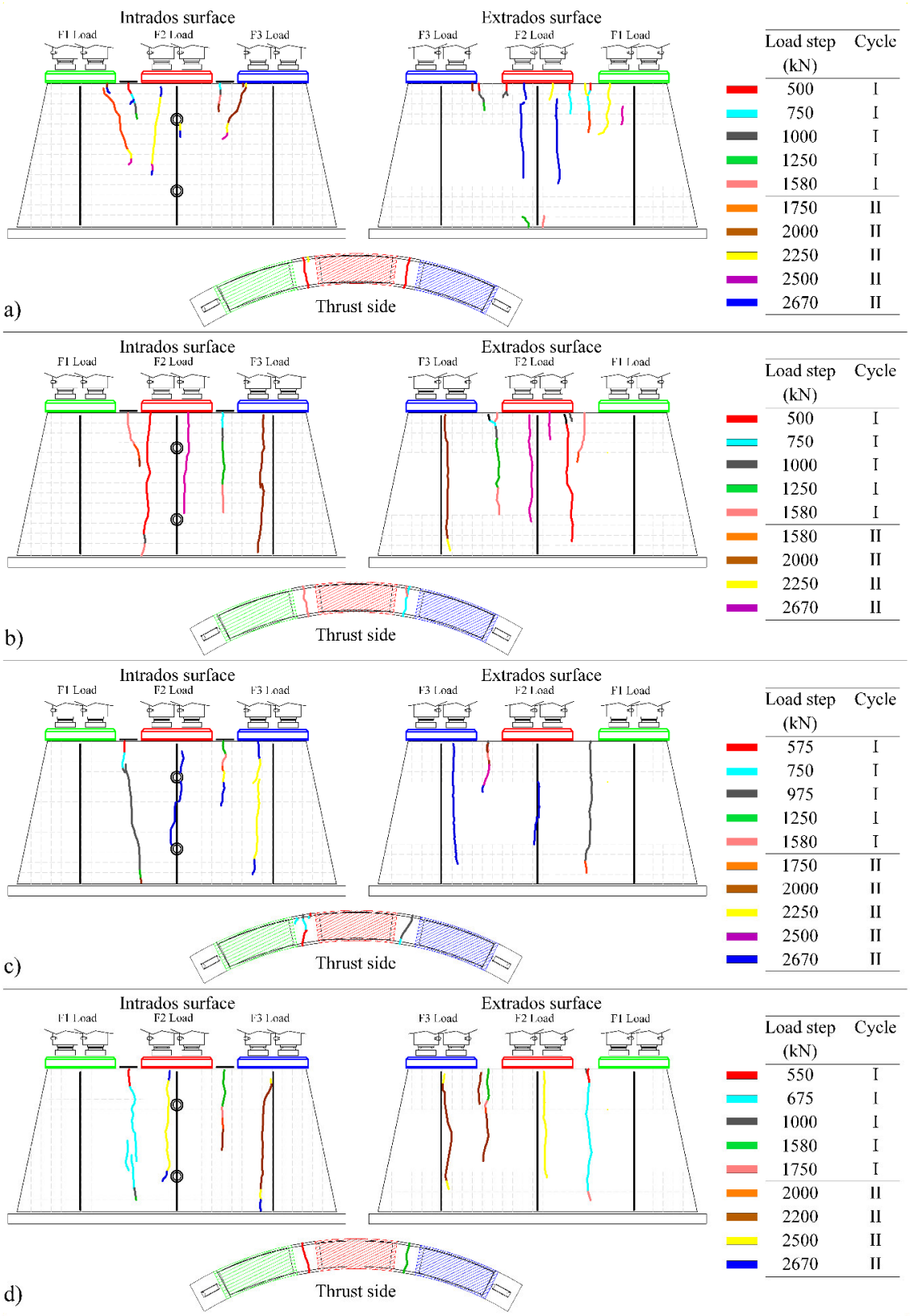

Figure 15. Point load test: crack pattern. a) SR; b) GFRP-RR; c) GFRP-LR; d) GFRP-WR.

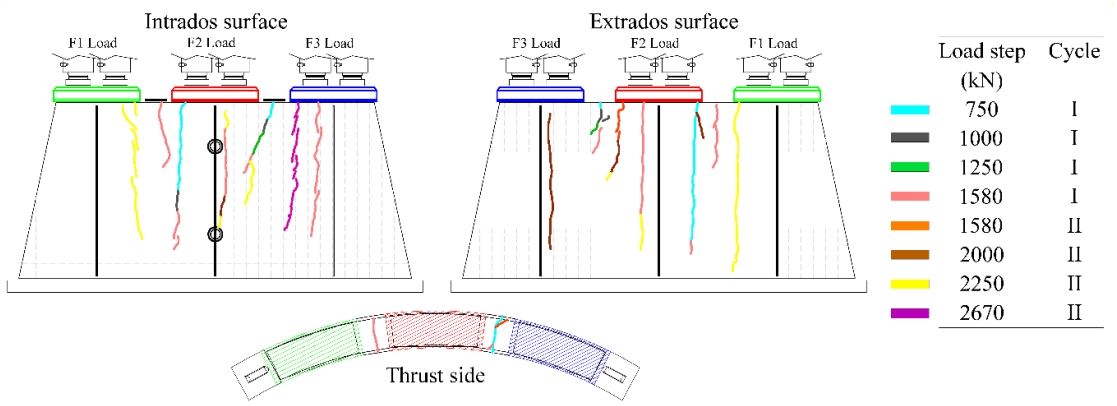

Figure 16. Point load test results: crack pattern of GFRP-RR(+B) segment.

Tables

Table 1. Design and experimental values of the material properties for the interaction diagrams definition.

Material	Property	Unit	
Concrete	Compressive strength	MPa	50
Steel	Tensile strength (yielding)	MPa	510
	Tensile modulus	GPa	210
GFRP	*E-CR fiber glass*		
	Density	g/cm^3	2.62
	Conductivity	W/m·K	1.22
	Pristine fiber tensile strength	MPa	3750
	Young's modulus	GPa	81
	Elongation at break	%	4.9
	CTE, 23-300 °C	x 10^{-6} °C^{-1}	6
	Impregnated strand		
	Tensile strength	MPa	2200-2600
	Tensile modulus	GPa	81
	Unidirectional composite		
	Tensile strength	MPa	1200
	Tensile modulus	GPa	48
	Poisson's ratio	-	0.33
	Fiber volume fraction	%	60
	Vinyl ester matrix		
	Density	g/cm^3	1.15-1.35
	Tensile strength	MPa	73-81
	Young's modulus	GPa	3.0-3.5
	Poisson's ratio	-	0.36-0.39
	CTE	x 10^{-6} °C^{-1}	50-75

Table 2. Failure modes of the segments.

Reinforcement	Failure mode	P_{crack} (kN)	w_{crack} (mm)	P_{max} (kN)	δ_{max} [(a)] (mm)	δ_y (mm)	δ_1 (mm)	μ (-)
SR	Rebars rupture[(b)]	145.0	0.10	471.7	56.7	7.7	-	7.4
GFRP-RR	Rebars rupture[(b)]	88.0	0.50	625.9	72.9	-	52.8	1.4
GFRP-LR	Rebars rupture[(b)]	107.5	1.30	550.7	71.8	-	50.9	1.4
GFRP-WR	Rebars rupture[(b)]	71.0	0.05	471.1	69.5	-	40.9	1.7

[(a)] δ_{max} calculated at 0.85 P_{max}. In this case, no collapse was seen at that point.
[(b)] The failure occurred for the achievement of the tensile strength by the intrados rebars

Table 3. GFRP-RR solution: comparison to the service load between reinforcements with and without bond treatment.

Reinforcement	Coating treatment	P_{crack} (kN)	w_{crack} (mm)	R_w (%)
GFRP-RR	None	88.0	0.50	-
GFRP-RR(+B)	Sand	106.7	0.15	70

Table 4. Point load test: maximum crack width.

	Loading cycle	SR	GFRP-RR	GFRP-LR	GFRP-WR	GFRP-RR(+B)	w_{max} [(e)]
w_{crack} (mm)	SL[(a)]	0.20	1.00	1.20	1.30	0.60	according to provisions
	UT[(b,c)]	0.35	1.25	1.50	2.00	1.20	
	UL[(d)]	0.15	0.40	0.70	0.70	0.25	0.50

[(a)] SL = Service load (1580 kN);
[(b)] UT = Unblocking thrust (2670 kN);
[(c)] For metro tunnel, TBM pushing capacity coincides with unblocking thrust; and
[(d)] UL = Unloding (0kN).
[(e)] w_{max} for RC segments with traditional steel reinforcement, according to the Codes, must be smaller than or equal to 0.30 mm.